Electronic Supporting Information to:

Co@NH_2-MIL-125(Ti): Cobaloxime-derived Metal-Organic Framework-based Composite for Light-driven H_2 Production

Maxim A. Nasalevich[1], René Becker[2], Enrique V. Ramos-Fernandez[3], Sonia Castellanos[1] Sergey L. Veber[4], Matvey V. Fedin[4], Freek Kapteijn[1], Joost N.H. Reek[2], Jarl Ivar van der Vlugt*[2] and Jorge Gascon*[1]*

[1]*Catalysis Engineering, Applied Sciences, Delft University of Technology, Delft, the Netherlands.*

[2]*Supramolecular and Homogeneous Catalysis, van't Hoff Institute for Molecular Sciences, University of Amsterdam, Amsterdam, the Netherlands.*

[3]*Laboratorio de Materiales Avanzados, Departamento de Química Inorgánica-Instituto Universitario de Materiales, Universidad de Alicante, Ap. 99, E-03080 Alicante, Spain*

[4]*Laboratory of Magnetic Resonance, International Tomography Center, Novosibirsk, Russia.*

Table of contents

1. Results and remarks

1.1. Nuclear magnetic resonance

1.1.1. Soluble compounds

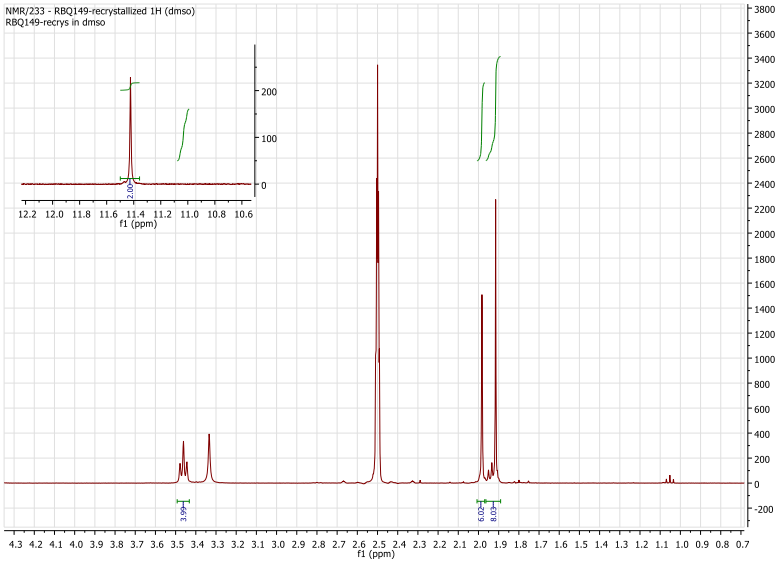

Figure S 1. ^{1}H-NMR spectrum of L^{H2} [(DOH)$_2$pn] in DMSO-d6. The small triplet at 1.05 ppm is of unknown origin.

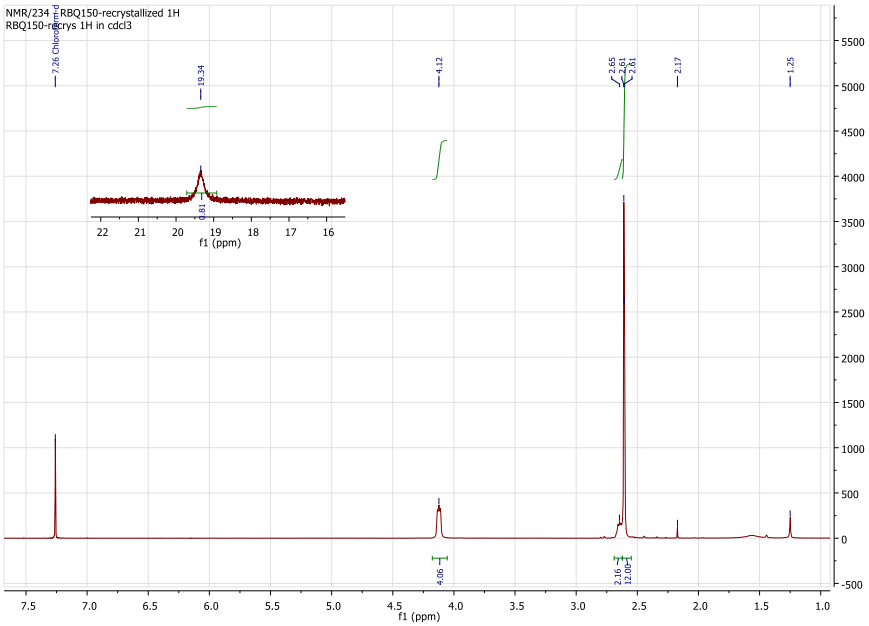

Figure S 2. ^{1}H-NMR spectrum of 1 [$Co^{III}Br_2L^{H}$] in $CDCl_3$. Note that singlets at 1.25 and 2.17 are from grease (Apiezon) and acetone, respectively.

1.1.2. Digested solids

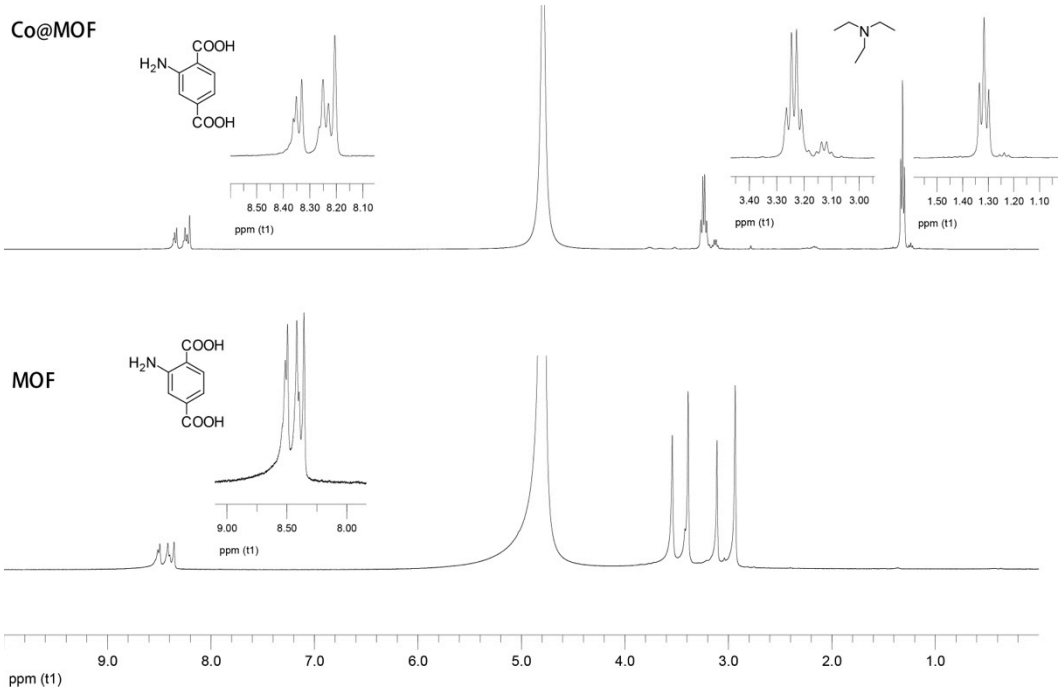

Figure S 3. ^{1}H-NMR of the aqueous phase after digestion with NaOD and neutralization with DCl. At the top: the quartet at 3.23 ppm and the triplet at 1.31 ppm are from TEA. At the bottom: singlets at 3.11 and 2.93 ppm are from DMF. Singlets at 3.54 and 3.39 ppm are attributed to products of DMF hydrolysis. The doublet:doublet:singlet system in 8.6-8.3 ppm is from the amino-terephthalate ligand. Slight changes in the pH values may produce shifts in the signals.

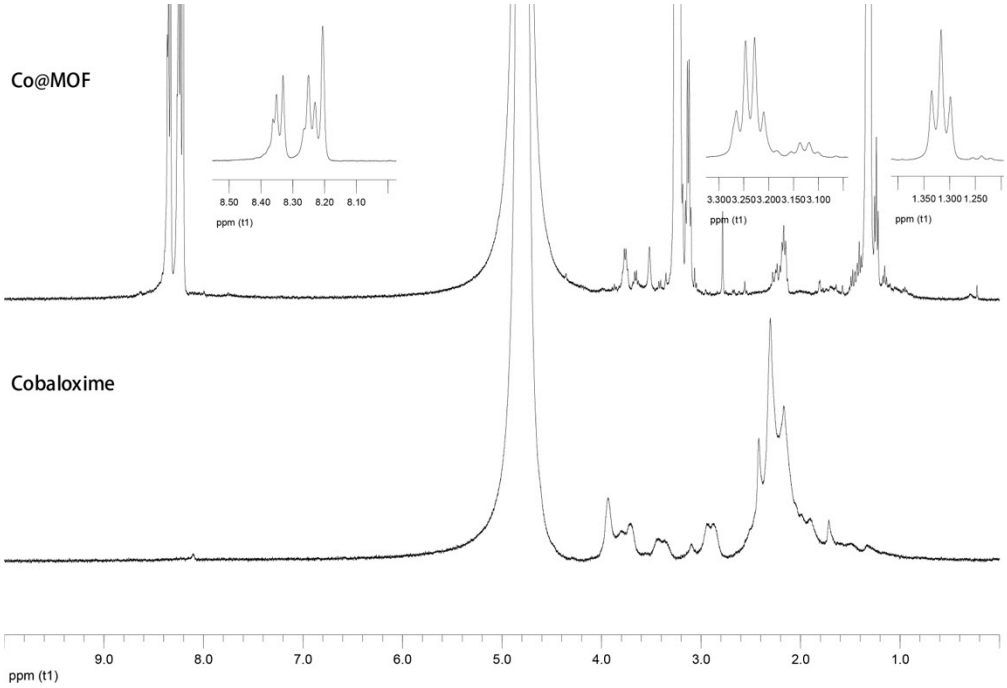

Figure S 4. ^{1}H-NMR of the aqueous phase after digestion with NaOD and neutralization with DCl.

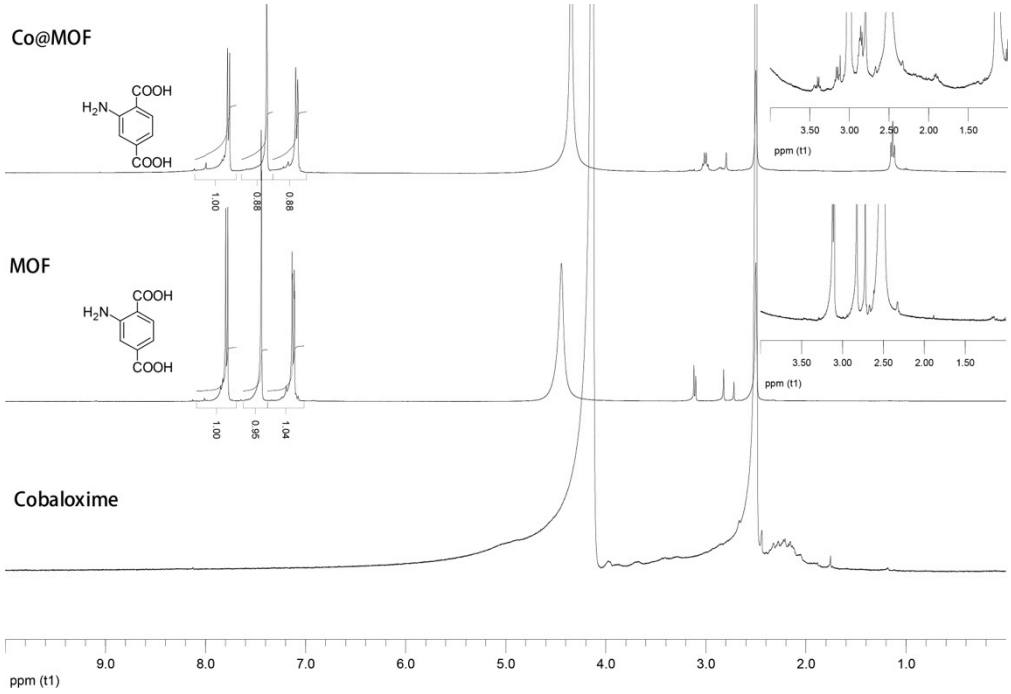

Figure S 5. ^{1}H-NMR of organic layer extracted with DMSO-d_6 from the digested samples. The doublet:singlet:doublet (1:1:1) system at 7.78, 7.44, and 7.13 ppm corresponds to the amino-terephthalate ligand. The broad signal around 4.50 ppm is from residual water.

1.2. UV/Vis spectroscopy (direct adsorption of 1 on MOF)

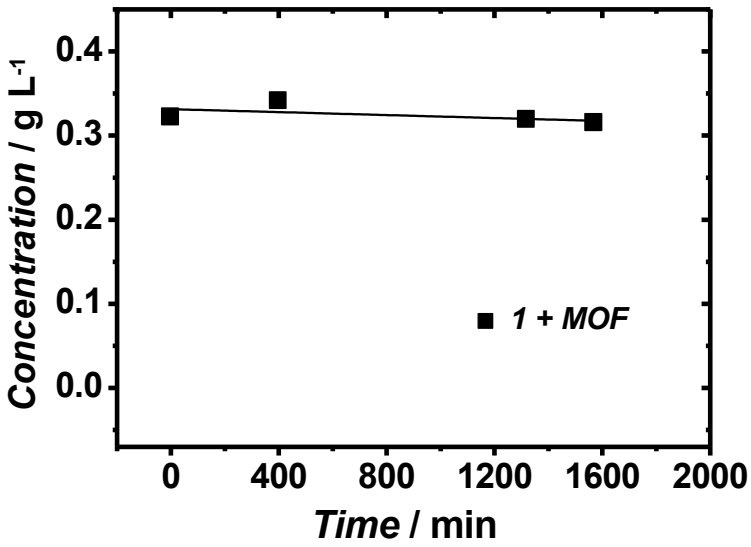

Figure S 6. Concentration of Cobaloxime 1 in contact with NH_2-MIL-125(Ti) in time followed by UV/Vis. Conditions: 45 mg MOF, 4 mg cobaloxime (1), 10 mL CH_3CN, 2 mL TEA, 0.2 mL H_2O, 1000 min^{-1}, RT.

1.3. Diffuse reflectance spectra of $CoBr_2$@MOF vs. Co@MOF

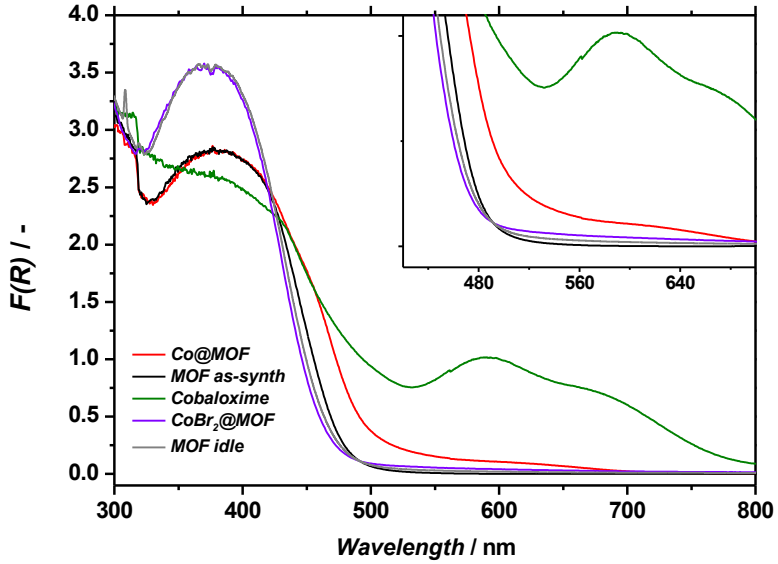

Figure S 7. DR UV/Vis spectra of Co@MOF (red), as-synthesized MOF (black), Cobaloxime 1 (olive), $CoBr_2$@MOF (violet), idle MOF (gray): the pristine MOF exposed to the same solvents as the $CoBr_2$@MOF sample.

As illustrated in Figure S7, the spectrum of $CoBr_2$@MOF synthesized as a blank, is substantially different from the one of the Co@MOF and resembles the spectrum of the MOF

exposed to the same solvents (acetone, CH_3CN, TEA, water). The only observed change as compared to the 'idle MOF' is a slight increase in the 500-700 nm region. However, in contrast to Co@MOF the band is ill defined and no additional band appears at 440 nm. Taking into account the quantity of $CoBr_2*6H_2O$ which was the same as in the case of the synthesis of Co@MOF, one can conclude that the newly appeared absorption bands of Co@MOF belong to the organometallic cobalt species within the composite and not to the species originating from the $CoBr_2$.

1.4. Tauc plots for NH_2-MIL-125(Ti) and Co@MOF

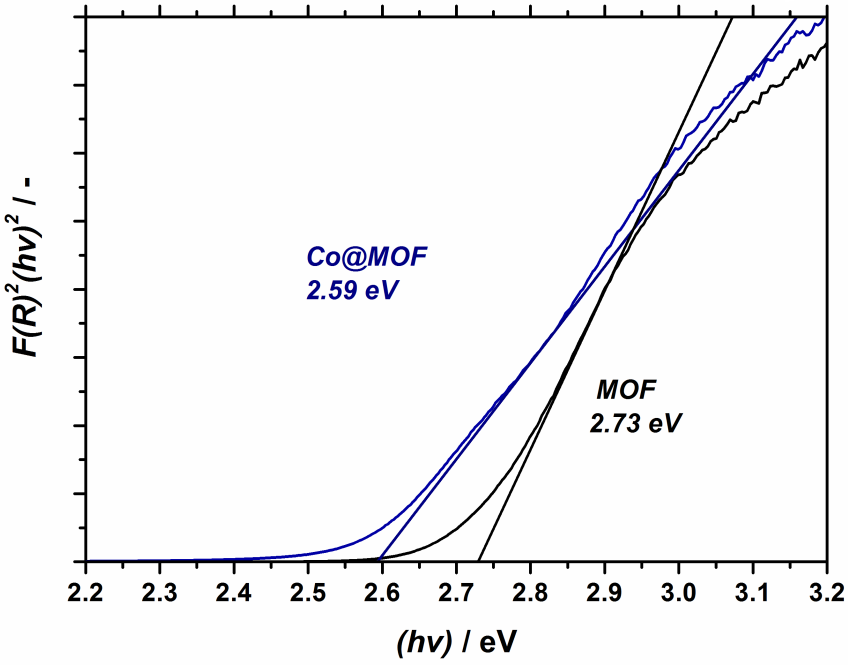

Figure S 8. Tauc plots for pristine NH_2-MIL-125(Ti) (black) and Co@MOF composite (blue) under the direct transition assumption.

The HOMO-LUMO gaps for NH_2-MIL-125(Ti) and Co@MOF were found to be 2.73 and 2.59 eV, respectively.

1.5. Fluorescence lifetime spectroscopy

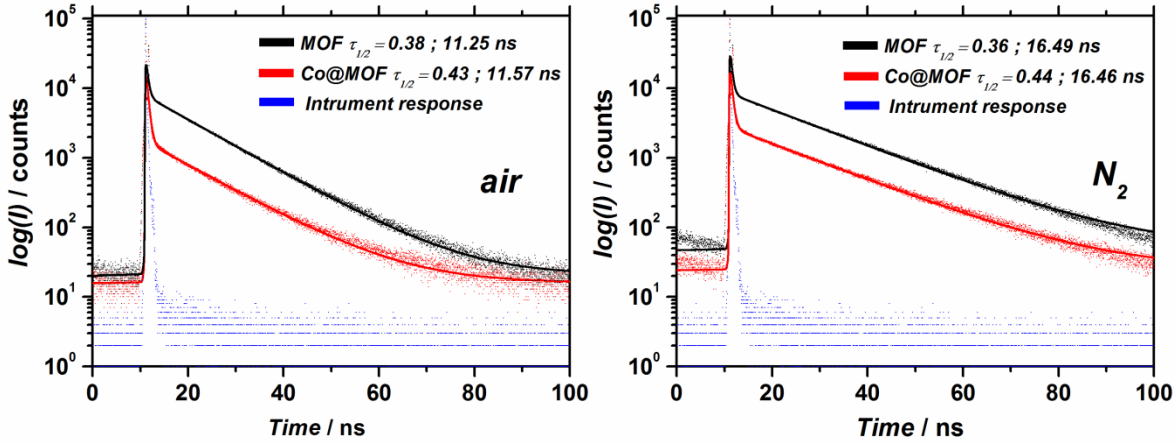

Figure S 9. Fluorescence lifetime spectroscopy for NH_2-MIL-125(Ti) (black) and Co@MOF composite (red) in air (left) and nitrogen (right). Conditions: 1mg in 10 mL CH_3CN suspension, emission observed at 440 nm.

Fluorescence lifetimes (τ) of NH_2-MIL-125 and the composite Co@MOF were measured by preparing suspensions of both materials in acetonitrile (0.01% w.) under air and after deoxygenating with N_2. Decays of fluorescence emission at 440 nm were biexponential in all cases, however lifetimes were longer in the absence of oxygen for the second component, τ_2. The very short characteristic decay time τ_1 = 0.4 ns is attributed to the inaccuracy of the instrument response function reconvolution. This conclusion is also supported by the fact that τ_1 is not affected by the atmosphere (air vs. nitrogen). Therefore, the meaningful fluorescence lifetimes are the ones denoted τ_2 and are equal for the pristine NH_2-MIL-125(Ti) (11.25 ns in air, 16.5 ns N_2 saturated) and Co@MOF (11.6 ns in air, 16.5 ns N_2 saturated.

It must be noted, that photocatalytic reduction of H^+ to H_2 can proceed through two different paths, as illustrated in Figure S10.[1] In path A (reductive quenching) the excited state of the photosensitizer (PS^*) is reduced by the sacrificial donor (SD) before electron transfer to the catalytic center (CC) occurs. In path B (oxidative quenching), electron transfer from PS^* to CC is the first step, followed by the regeneration of the resulting hole in the photosensitizer (PS^+) to the initial species.

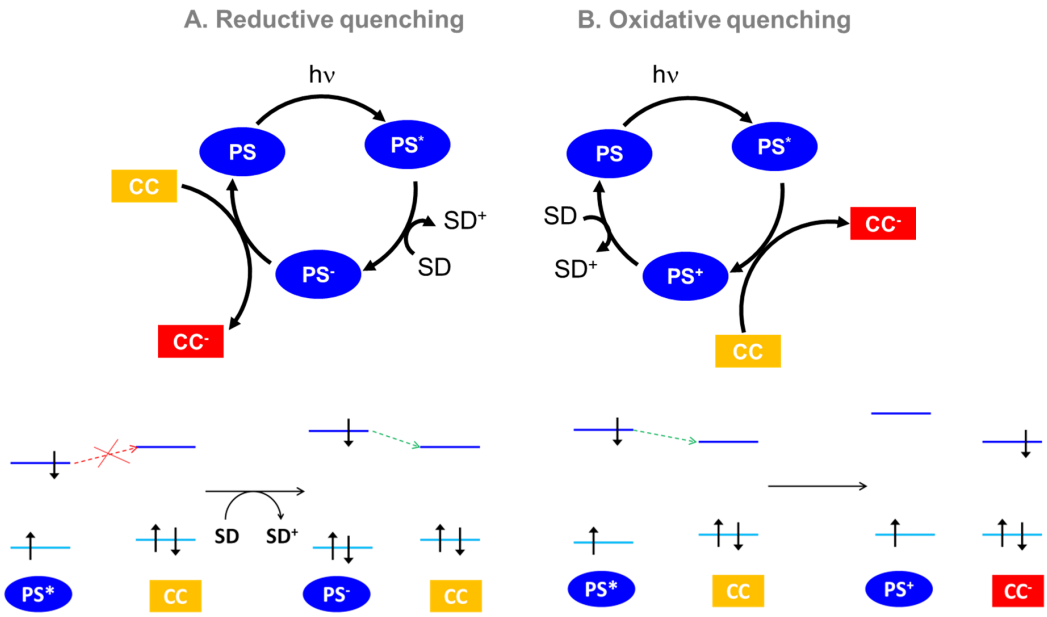

Figure S 10. Scheme of two different mechanisms (A and B) for photoinduced electron transfer from a photosensitizer (PS) to a catalytic centre (CC) using a sacrificial donor (SD) as electron source (inspired by Artero et al.[1]). At the bottom, schematic representations of the frontier orbital levels for PS and CC during the two processes. For simplification, kinetic effects (activation energies) are not considered in the figure.

In the particular case of Co@MOF, NH_2-MIL-125 acts as the photosensitizer (PS), cobaloxime as the catalytic center (CC), and TEA as the sacrificial donor (SD). Given, the absence of shortening in τ in the presence of cobaloxime, it seems reasonable to think that photoinduced generation of H_2 in Co@MOF proceeds through the reductive quenching of the MOF. That is, the electron transfer to the cobaloxime cannot occur from NH_2-MIL-125 in the excited state but from the reduced form of the MOF. For this reason, the presence of the Co complex does not affect the fluorescence lifetime of NH_2-MIL-125 (the radiative relaxation does not have a competing oxidative pathway). Another possible explanation for the observed lifetimes can be a kinetic effect associated with the rate of fluorescence versus the rate of electron transfer. If the former one is much faster than the latter one, no change in fluorescence lifetime can be expected in case of cobaloxime inclusion.

In contrast, and further supporting our hypothesis, in the EPR studies (see section 3.4 in the manuscript) when TEA was used as sacrificial donor the EPR signal corresponding to Ti^{III} of NH_2-MIL-125 is detected upon irradiation. However, in the presence of Co@MOF this signal fades and a new band assigned to Co^{II} appears instead. Thus, upon irradiation, TEA transfers electrons to the excited MOF, which can be further transferred to the cobaloxime.

Artero and colleagues summarized in their recent review that both, the reductive quenching and the oxidative quenching, may occur when cobaloximes are used as catalytic sites. The

mechanism type depends on the cobalt oxidation state, organic dye used as a photosensitizer, electron donor concentration etc.[1]

1.6. TEM and EDX

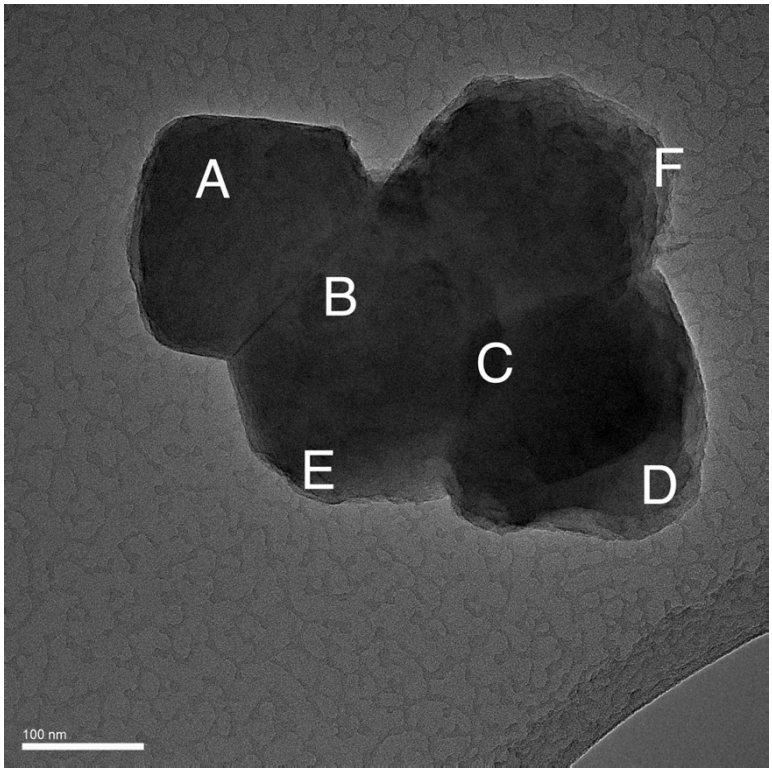

Figure S 11. HRTEM image of Co@MOF catalyst.

Table S 1. Integrated EDX peak areas of various regions within Co@MOF catalyst crystallite.

Region	Integrated Ti signal / a. u.	Integrated Co signal / a.u.	Co/Ti ratio
A	2866	107	0.04
B	3221	257	0.08
C	3568	213	0.06
D	3456	221	0.06
E	2806	120	0.043
F	3002	170	0.06
The entire particle	2696	165	0.06

1.7. SEM and EDX

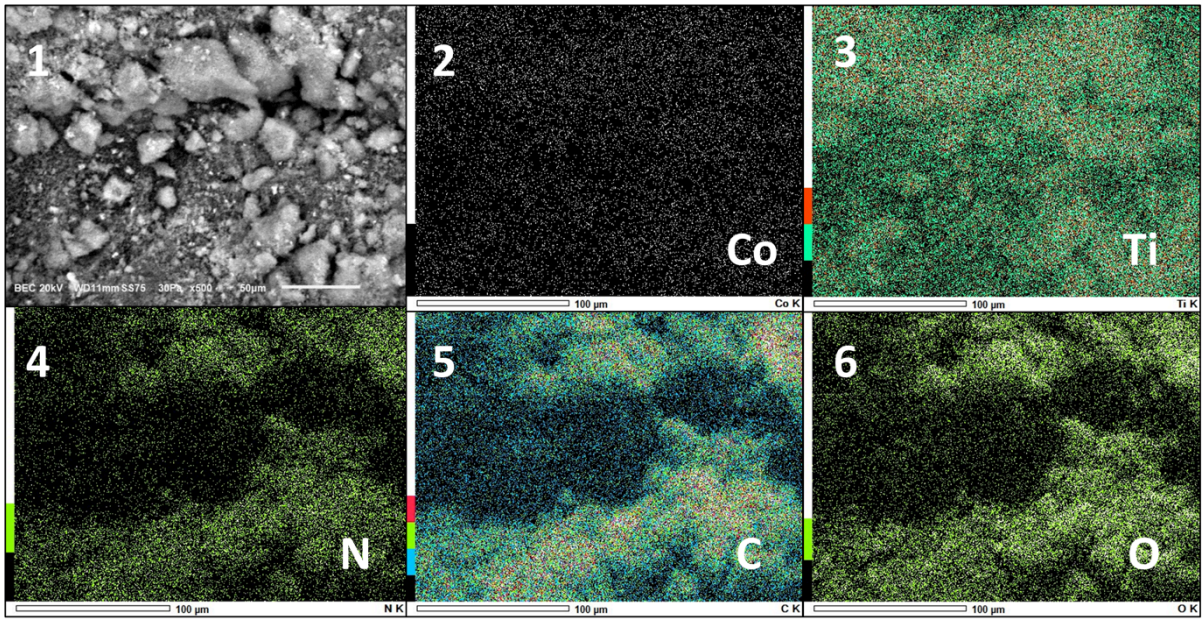

Figure S 12. SEM EDX studies on Co@MOF composite: (1) SEM image at 500x magnification; EDX mapping for (2) Co; (3) Ti; (4) N; (5) C; (6) O. The scale bar for SEM image is 50 µm and 100 µm for mapping.

1.8. Mass-spectrometry

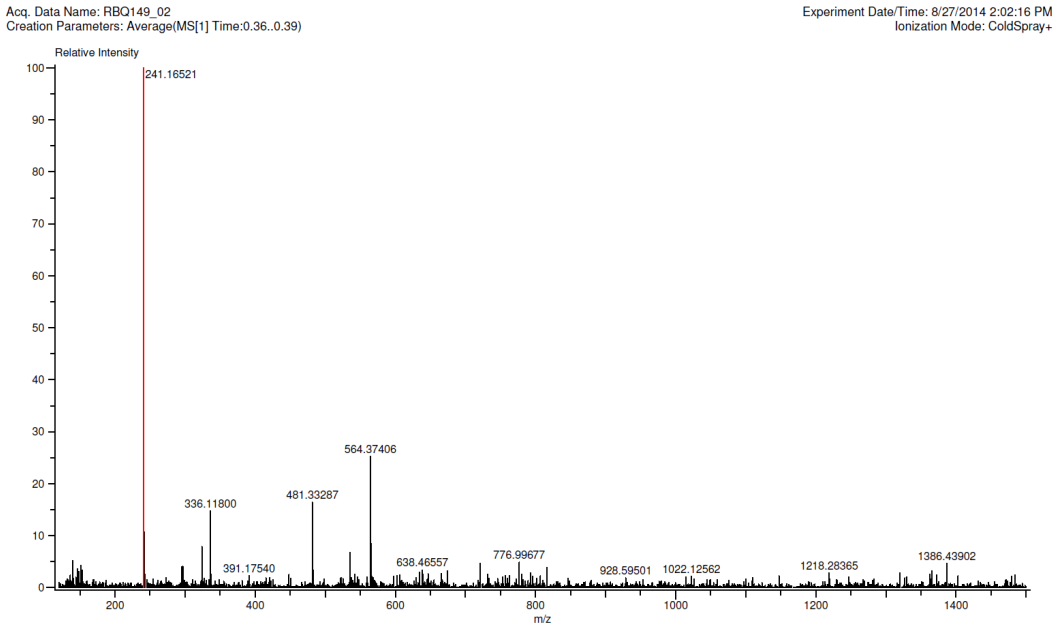

Figure S 13. Mass spectrum of $(DOH)_2pn$, the precursor for the formation of 1. The red vertical line denotes the molecular weight of the ligand.

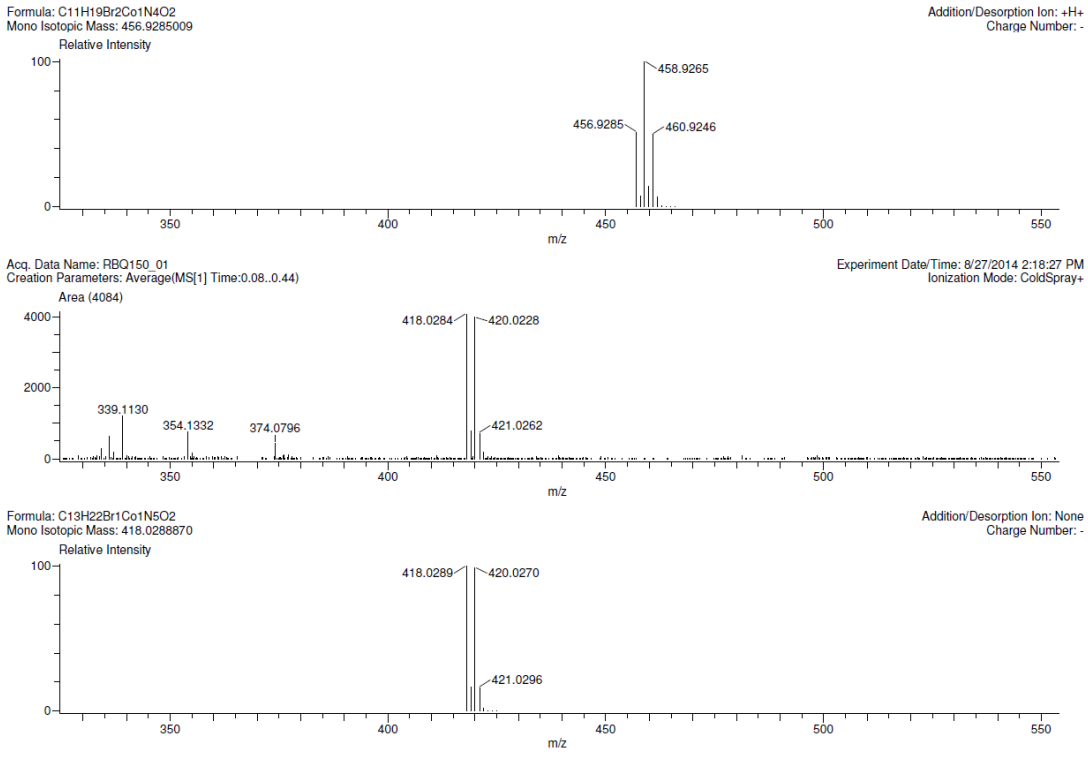

Figure S 14. Experimental mass spectrum of Cobaloxime 1 dissolved in CH_3CN (middle). Simulated spectra of intact (top) and CH_3CN (bottom) substituted Cobaloxime 1. The experimental pattern matches the one of the CH_3CN substituted 1.

1.9. Comparison of Co@MOF with literature

MOF systems

Table S 2. Comparison of Co@MOF composite with MOF-based photocatalytic systems reported in literature.

Catalyst	*Photosensitizer*	*TON / -*	*initial TOF / h^{-1}*	*Light source*	*Sacrificial agent*	*Reference*
$Fe_2(\mu\text{-dcbdt})(CO)_6$ (covalent to UiO-66)	$Ru(bpy)_3$[c] (solution)	5.9 (d/a)[a]	6.8	470 nm	Ascorbic acid	Ott et al., *J. Am. Chem. Soc.* **2013**, *135*, 16997 [2]
Pt^0-NP (deposited)	NH_2-MIL-125	47.6[b] (d/a)	6.5	> 420 nm	TEOA	Matsuoka et al., *J. Phys. Chem. C* **2012**, *116*, 20848 [3]
$Pt(bpy)Cl_2$ (coordinated)	MOF-235	5.3 (d/a)	0.19	> 420 nm	TEOA	Xu et al., *Energy Environ. Sci.* **2013**, *6*, 3229 [4]
Cobaloxime **1**	NH_2-MIL-125	52	0.8	> 408 nm	TEA	This work
Pt^0-NP (solution)	Al-PMOF	0.8 (based on Pt)	0.1	> 420 nm	EDTA	Rosseinsky et al., *Angew. Chem. Int. Ed.* **2012**, *51*, 7440 [5]
Pt^0-NP (deposited)	$Ir^{III}(ppy)_2(bpy)$ (covalent to UiO-67)	7000 (ir) 389 (Pt) (d/a)	270 (Ir) 15 (Pt)	> 420 nm	TEA	Lin et al., *J. Am. Chem. Soc.* **2012**, *134*, 7211 [6]

As it can be seen, most of the MOF-based systems employed for hydrogen production up to date deactivate in time and contain various noble metals, whereas the system reported in this work is fully based on earth-abundant elements, stable in time and exhibits reasonable *TOF*.

Homogeneous systems using cobaloxime 1

Table S 3. Overview of homogeneous photocatalytic systems containing cobaloxime 1.

Photosensitizer	*TON / -*	*initial TOF / h^{-1}*	*Light source*	*Sacrificial agent*	*Reference*
$Ir(ppy)_2(bpy)$	696 (d/a)	154	> 400 nm	TEA	Artero et al., *Inorg. Chem.* **2012**, *51*, 2115 [7]
$Ru(bpy)_3$	4	?	> 400 nm	Ascorbic acid	Collomb et al., *Phys. Chem. Chem. Phys.* **2013**, *15*, 17544 [8]
$Re(py)(bpy)(CO)_3$	93 (d/a)	2.2	380 nm	TEOA	Alberto et al., *Eur. J. Inorg. Chem.* **2012**, *1*, 59 [9]

Not many homogeneous photocatalytic systems based on cobalt diimine-dioxime are known. Although the rhenium-based systems of Alberto *et al.* are very promising candidates, they still tend to deactivate fast.

a: d/a = deactivation reported.

b: The *TON* calculation was based on the assumption that Pt was quantitatively deposited on NH_2-MIL-125(Ti). It should be noted that at the reaction conditions of Matsuoka et al. the hydrogen evolution rate for Pt@NH_2-MIL-125(Ti) was found to be double the one of pristine NH_2-MIL-125(Ti) whereas in this work this comparison yields 20-fold enhancement.

c: The main drawbacks of the reviewed systems are highlighted red: use of precious metals, system deactivation, low turnover frequency.

1.10. Recycling tests

Recycling tests were performed using a typical **Co@MOF** sample (intermediate Co-loading) using the procedure stated in paragraph 2.5 of the main text. After approximately 23 hours of operation, the catalyst was recovered as stated and used as such for the next run.

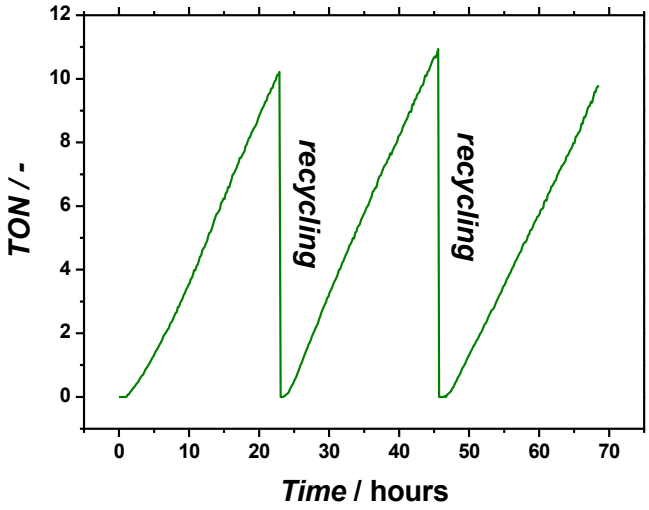

Figure S 15. Recycling tests for Co@MOF.

The steady-state hydrogen evolution rates for the three subsequent runs were 0.81, 0.76 and 0.73 µmol/hr respectively. Since during recycling some material is inevitably lost, we conclude there is no *appreciable* deactivation even after 68 hours of operation.

1.11. Addition of $CoBr_2$ to the working catalyst

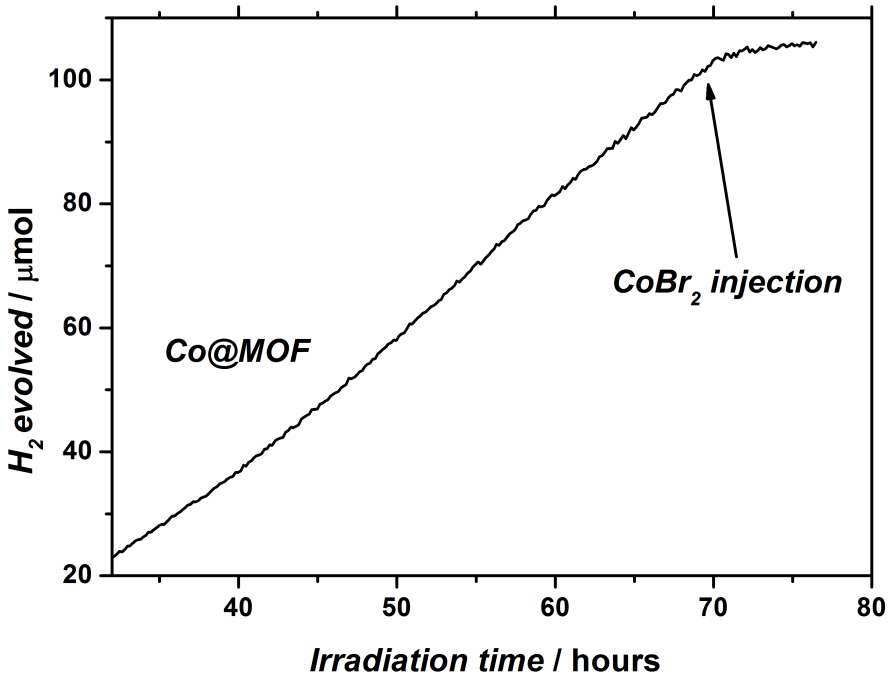

Figure S 16. Inhibition of hydrogen production by adding $CoBr_2$ solution in CH_3CN to the working Co@MOF catalyst.

1.12. Diagram of redox potentials of building blocks of Co@MOF composite

In order to illustrate the theoretical feasibility of the assembly design presented in this work we envisioned a diagram shown in Scheme 3 of the main text. As mentioned in the manuscript the HOMO-LUMO levels of NH_2-MIL-125(Ti) were extracted from the recent paper by Walsh and colleagues in which they predicted the potentials for MIL-125(Ti) in vacuum.[10] Earlier Walsh has shown that HOMO of MIL-125(Ti) is mainly localized at the organic linker, terephthalic acid, while LUMO resides primarily at the inorganic secondary building unit, Ti-oxocluster, while by changing the linkers one can tune the HOMO-LUMO gap of the materials of this series.[11] Based on this work it seems logical to assume that changes in the substituents of the aromatic system of the linker should mainly cause changes in HOMO of MIL-125(Ti) whereas LUMO residing at the inorganic cluster remains nearly unchanged. Following this rationale we calculated the redox levels to be 7.6 eV vs. vacuum and 3.8 eV for HOMO and LUMO, respectively. The energy of HOMO was calculated taking into account the difference in HOMO-LUMO gaps of NH_2-MIL-125(Ti) and MIL-125(Ti) (2.6 eV vs. 3.8 eV) and keeping the LUMO level constant. The assumptions undertaken are also supported by the fact that NH_2-MIL-125(Ti) was reported to catalyse hydrogen evolution[3] evidencing the thermodynamic suitability of the material (H^+/H_2 reduction potential is generally accepted to be around 4.4 eV vs. vacuum).

The catalytic potential illustrated in Scheme 3 corresponds to experimental data reported by Fontecave and co-workers for the first cobalt reduction potential.[12] Once the potential is reached the catalytic cycle starts although one should note that the mechanism behind hydrogen evolution by cobaloximes is more complex and is beyond the scope of this work. The experimental data was referred vs. ferrocene couple. The cobalt redox level was then converted to the level vs. vacuum using the following equation:

$$E_{LUMO} = -(E_{red} + 4.8)$$

Importantly, the potentials summarized in Scheme 3 can only be seen as a very rough approximation and are presented to demonstrate the theoretical feasibility while they shouldn't be relied on. First of all, calculated values shouldn't be compared with the experimental results since the calculated data does not contain information of the solvent effects and pH dependency of the redox potentials. Secondly, the exact structure of cobaloxime **1** within the pores of NH_2-MIL-125(Ti) is likely to be different than in the case of the molecular compound in solution as is evident from several experimental techniques such as EPR.

1.13. Calculation of external quantum efficiency

External quantum efficiency can be defined by the following expression:

$$\Phi = \frac{E(t)}{P(t)} \qquad (1),$$

where *E(t)* is a number of electrons carrying out a redox reaction per unit of time; *P(t)* is a photon flux per unit of time.

The best performing Co@MOF catalyst demonstrated the hydrogen evolution rate of 3.1 μmol(H_2) h^{-1}. However, in order to produce 1 molecule of H_2 gas one would need 2 electrons. Therefore the numerator in the expression (1) becomes 6.2 μmol electrons h^{-1}.

The intensity of the light source used in this study was determined using an AvaSpec-3648-2-USB2 (Avantes, the Netherlands). Figure S17 shows light intensity at the lamp focal point (50 cm) as a function of wavelength:

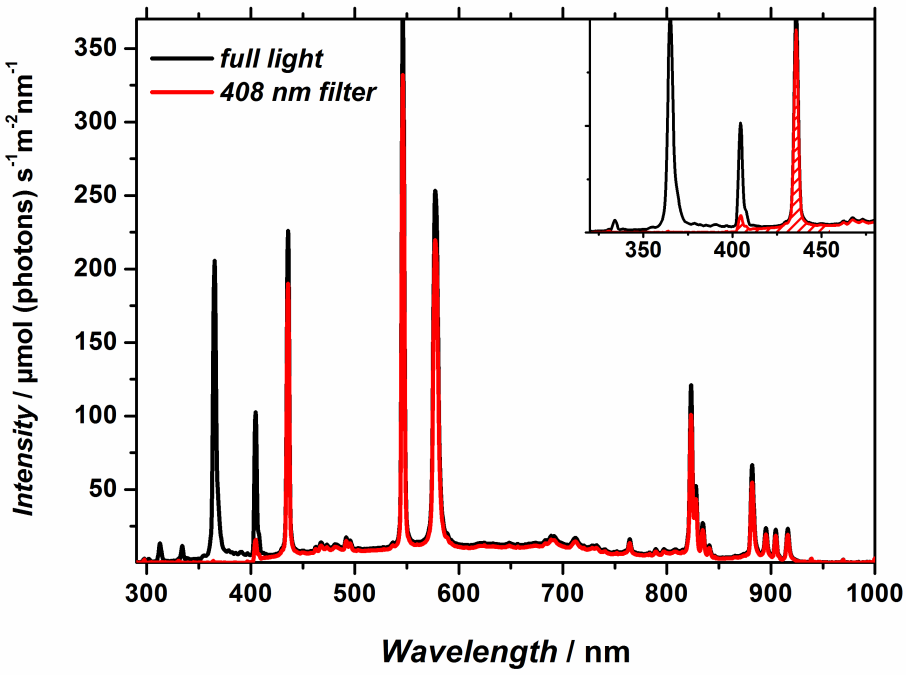

Figure S 17. Spectrum of the 500W Xe/Hg ligh source utilized in this study at focal point (50 cm). Unfiltered light (black) and 408 nm cut-off filtered light (red). The filled area in the inset represents the integral over the operation range for the current photocatalytic system (408 nm – 455 nm).

After integrating the curve obtained by applying the 408 nm cut off filter and taking into account the charge transfer mechanism proposed in this work and the HOMO-LUMO gap of NH_2-MIL-125(Ti) (2.73 eV = 455 nm) a total integral lamp intensity over the 350 – 455 nm range becomes 883.6 µmol(photons) $s^{-1}m^{-1}$. One should note that the integration was performed over 350 – 455 nm to ensure the claimed filter cut-off wavelength. Indeed, below 400 nm the intensity of the light source goes to 0.

The illuminated area was 4.2 cm^2 and thus P(t) = 883.6*3600/10000*4.2 = 1336 µmol (photons) h^{-1}

$$\Phi = \frac{E(t)}{P(t)} = \frac{6.2\mu mol(electrons)h^{-1}}{1336\mu mol(photons)h^{-1}} = 0.00464 \approx 0.5\%$$

1.14. Calculation of apparent activation energy

The apparent activation energy of hydrogen production using Co@MOF composite was obtained by measuring reaction rates at two different temperatures: 278 K and 297 K. Our efforts to vary temperature over a wider range met with practical limitations. Performing photocatalytic tests at temperatures lower than 5 ^{0}C is not possible due to the limitations of the reactor design, while heating the reaction mixture at 40 ^{0}C led to significantly lower reaction rate, presumably due to the excessive evaporation of volatile TEA as the electron

donor. As a result, we herein present what should be considered an indicative value for the apparent E_{act}. The following equation was obtained for the two reaction rates measured at 278 K and 297K:

$$\ln(R) = 15.3 + 0.4(-1/k_B T)),$$

Where R – reaction rate [μmol h^{-1}]; T – temperature [K]; k_B – Boltzmann constant.

The apparent activation energy was extracted from the slope of the linear function and was found to be 0.4 eV. The reaction rates used for the calculation were obtained by letting the reaction run for at least 8 hours to ensure the steady-state rate for both temperatures.

1.15. Washing protocol

All Co@MOF composites employed in this work were washed prior to the exposure to visible light. The as-synthesized catalysts were dispersed in a CH_3CN/TEA/H_2O similar to that under photocatalytic conditions. The suspension was kept in the dark under stirring overnight, then filtered. The powder was washed with two portions of acetone. Such protocol was developed based on the observation made at the earlier stages of the development of this work. It was noticed that as-synthesized catalysts possess lower activity than the catalysts exposed to the conditions described above as shown in Figure S18:

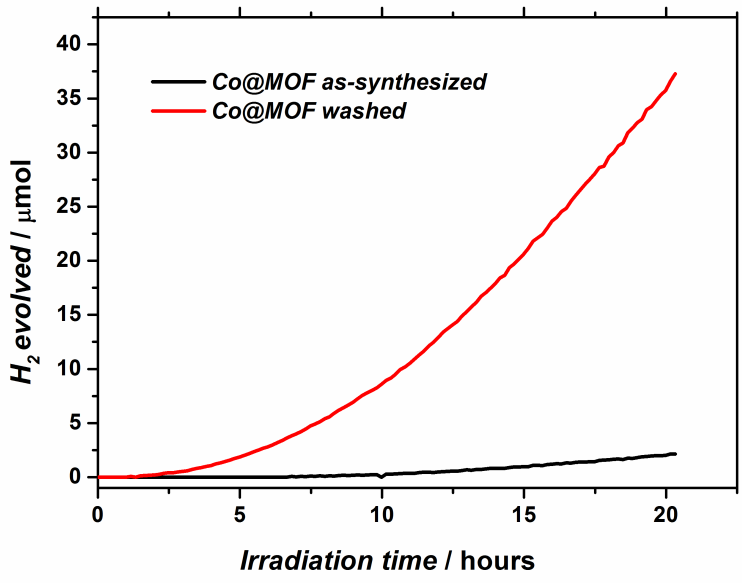

Figure S 18. Photocatalytic activity towards hydrogen for as-synthesized (black) and washed (red) Co@MOF composite.

Later EPR spectroscopy on the as-synthesized and washed catalysts demonstrated that desorption of $CoBr_2$ impurities takes place during this washing step (Figure S19).

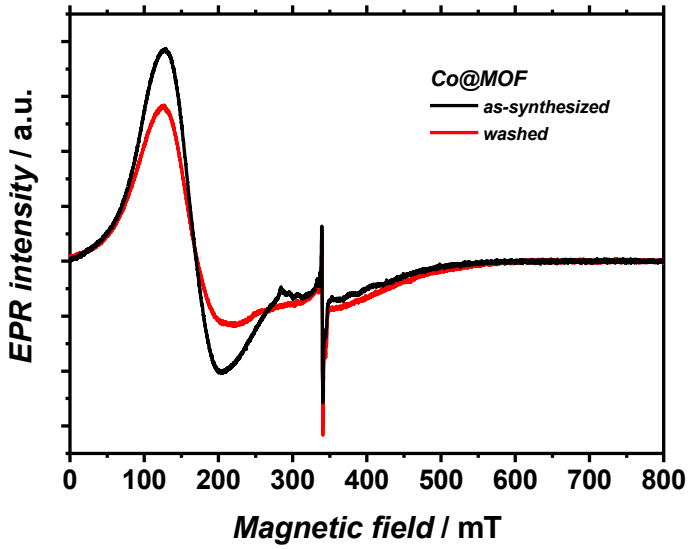

Figure S 19. CW EPR spectra of as-synthesized (black) and washed (red) Co@MOF composite. The spectra were recorded in X-band at temperature 40 K and mw frequency 9.55 GHz.

1.16. Electron Paramagnetic Resonance

I. General experimental and simulation procedures

All experiments have been done using commercial X/Q-band EPR spectrometer Bruker Elexsys E580, equipped with Oxford Instruments temperature control system. The compounds were placed into the quartz sample tubes and sealed, and all experiments have been carried out at X-band microwave frequency in Continuous Wave (CW) mode. For room-temperature irradiation, the 500 W high-pressure mercury lamp equipped with a 420 nm cut-off filter has been used.

The simulations were done using the EasySpin toolbox for Matlab[13, 14]

II. **Experimental and simulated EPR spectra of $CoBr_2$ in CH_3CN**

The experimentally observed shape of the X-band EPR spectrum of $CoBr_2$ implies that the complex is found in the high-spin state with the zero-field splitting (ZFS) significantly exceeding the energy of the microwave quantum ($D>>h\nu_{mw}$). In such situations, instead of common resonances in the central magnetic field (g~2) typical for low-spin Co^{II}, the signals around g~4 are observed corresponding to the perpendicular components of the g-tensor. This is exactly the trend observed by us for $CoBr_2$ in CH_3CN, therefore we safely conclude that Co^{II} ion is found in the high-spin state with total spin **S**=3/2.

Good agreement between experimental and simulated spectra (Figure S20) can be obtained using spin Hamiltonian of the quartet state (**S**=3/2) of high-spin Co^{II} complex [Eq. S1]:

$$\hat{H} = \beta\mathbf{BgS} + D\left(S_z^2 - S(S+1)/3\right) + E(S_x^2 - S_y^2) + \mathbf{SAI} \qquad \text{(S1)},$$

where $\mathbf{B} = [0, 0, B]$ is the magnetic field along the z-axis; **g**=[2.4, 2.4, 2.0] is g-tensor of Co^{II} ion; $D \geq 1800$ mT and E=0 mT are the parameters of the zero-field splitting (ZFS) tensor; and **A**=[0, 0, 16] mT are the components of the hyperfine interaction (HFI) tensor.

Identical spectrum to that shown in Figure S20 can be obtained in the model of the effective spin **S**=1/2 using spin Hamiltonian:

$$\hat{H} = \beta\mathbf{BgS} + \mathbf{SAI} \qquad \text{(S2)},$$

where A-tensor has the same values **A**=[0, 0, 16] mT, and the effective g-tensor is $\mathbf{g}^{eff}$=[4.8, 4.8, 2.0]. In both cases the Voigtian broadening (Gaussian + Lorentzian) of EPR lines was used with Γ_{pp}=5 mT (peak-to-peak) for Gaussian and Γ_{pp}=25 mT for Lorentzian lineshape.

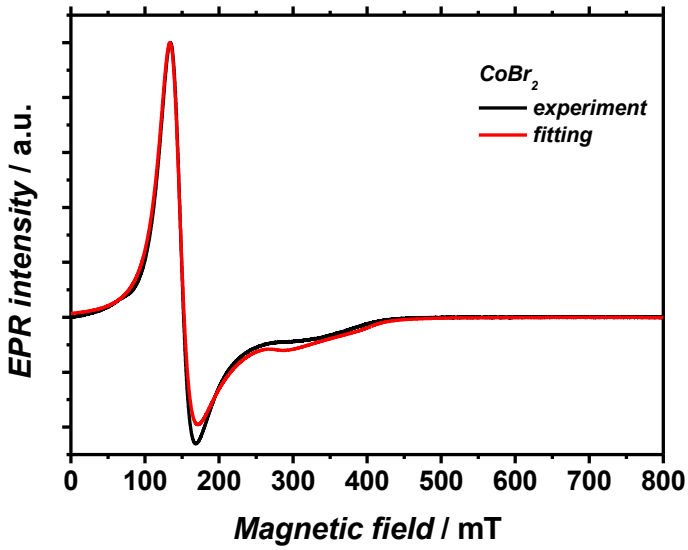

Figure S 20. Experimental (black) and simulated (red) CW EPR spectra of $CoBr_2$ dissolved in CH_3CN. Experimental spectrum was recorded in X-band at temperature 40 K and mw frequency 9.5512 GHz. Parameters of spin Hamiltonian used in simulation are given in the text.

Since the obtained *g*-tensor is axially symmetric ($g_x = g_y$) and the E parameter of ZFS equals to zero, one assumes closely axial symmetry of the Co^{II} ion environment. The values of *g*-tensor are typical of six-coordinated octahedral high-spin Co(II) complexes with tetragonal distortion,[15, 16] therefore the investigated $CoBr_2$ complex dissolved in CH_3CN is believed to exhibit closely axial symmetry with the Co-Br bonds longer compared to Co-N.

III. Experimental and simulated EPR spectra of photo-generated Co^{II} species within the Co@MOF catalysts.

Experimental EPR signal of Co^{II} species within the Co@MOF composite is shown in Figure S21 (black). It shows a single and very broad line, which is not expressive and does not possess distinct features. As has been explained above for $CoBr_2$, the spectrum of high-spin Co^{II} complex can be simulated using true spin Hamiltonian of the quartet state **S**=3/2, or, alternatively, using model spin Hamiltonian **S**=1/2. The available literature data for high-spin Co^{II} complexes often operates with the values of effective g-tensor (**S**=1/2 model), therefore for convenience of comparison we also simulate signal of photoinduced Co^{II} species using **S**=1/2 spin Hamiltonian (2S) (Figure S21, red).

Good agreement between experiment and calculation can be obtained using $\mathbf{g}^{eff}$=[6.0, 2.4, 1.7] and *A*=0. The experimentally observed lineshape is essentially Gaussian, and can be simulated using 200 mT broadening (peak-to-peak). Deviations between experimental and simulated spectra in the low magnetic field are mainly caused by

additional EPR signal ($CoBr_2$ admixtures) present in the 'dark' spectrum (see Figure 9C for details).

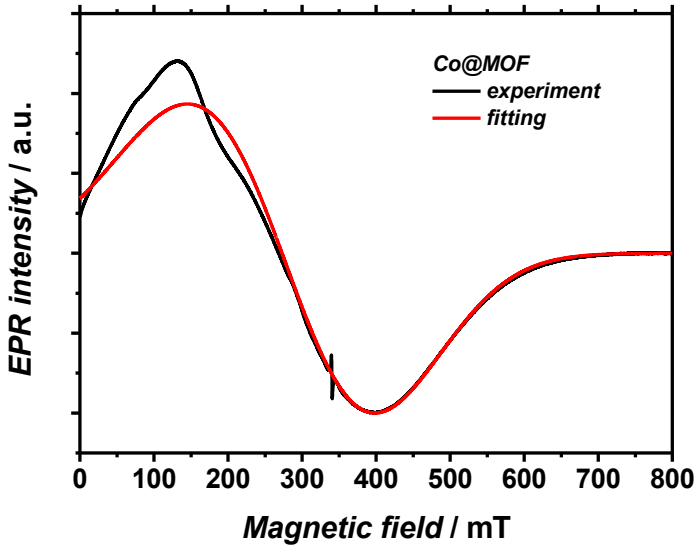

Figure S 21. Experimental (black) and simulated (red) CW EPR spectra of Co^{II} species within Co@MOF. Experimental spectrum was recorded in X-band at temperature 40 K and mw frequency 9.5533 GHz. Parameters of spin Hamiltonian used in simulation are given in the text.

The strong broadening of the experimental spectrum does not allow us to conclude on the exact values of *g*-tensor and, as a result, the geometry of the complex. In principle, a rather broad range of *g*-tensors would allow for reasonable fitting. However, one should also consider the connection between g-tensor components and the rhombicity of the ZFS tensor (*E/D*) found for high-spin Co^{II} ions in octahedral environment[15]. Taking this into account, we have found that the use of g-values characteristic for axially symmetric high-spin Co^{II} complexes does not allow for satisfactory agreement between experimental and simulated spectra. In contrast, assuming rhombic distortion of Co^{II} octahedron and ZFS tensor ($E=D/3$), good agreement between experimental and simulated spectrum can be obtained. The obtained values $\mathbf{g}^{eff}$=[6.0, 2.4, 1.7] are consistent with the results of Luchinat and co-workers[15] and imply that E/D~1/3. Thus, although a strong broadening of the available experimental spectrum does not allow us to obtain definite parameters of *g*- and *D*-tensors, we safely conclude that (i) the observed Co^{II} species is high-spin, and (ii) it can be simulated using reasonable and self-consistent set of parameters.

The nature of strong broadening of the photoinduced Co^{II} species compared to $CoBr_2$ needs further investigation. As has been mentioned above, the lineshape of $CoBr_2$ is mainly Lorentzian, whereas it is mainly Gaussian for photoinduced Co^{II} complex. Gaussian line shape indicates inhomogeneous broadening of the spectrum due to the overlap of unresolved components. Most often Gaussian line shapes are caused by a distribution of magneto-resonance parameters in the investigated compounds, arising

possibly due to the conformational disorder. In the present work, such disorder may result from encapsulation of cobalt complex in MOF, and it is also coherent with the lower symmetry of magnetic tensors in encapsulated complex compared to free $CoBr_2$. Thus, the two observations found for photoinduced Co^{II} species (lower symmetry of magnetic tensors and broader Gaussian-shaped line) can be ascribed to the conformational disorder introduced by MOF confinement.

Finally, the quantitative analysis of the EPR data was done using second integrals of the baseline-corrected experimental signals. Double integration showed that the signal intensity of the catalyst in the dark was ~ $1.9 \cdot 10^{11}$ a.u., while the intensity of the sample exposed to illumination for 29 hours was ~ $2.9 \cdot 10^{12}$ a.u. So, the integral intensity of the EPR signal after irradiation increased by a factor of ~14. Assuming that the spin state of Co^{2+} species is the same in both cases (**S** = 3/2), one concludes that the total number of Co^{2+} species increased by the same factor of 14.

IV. Experimental spectrum of reduced Cobaloxime 1

In this experiment **1** containing Co^{3+} was reduced with Cobaltocene, $Co(Cp)_2$, under oxygen-free atmosphere directly in an EPR tube. The sample was cooled down to 12K and the spectrum acquired:

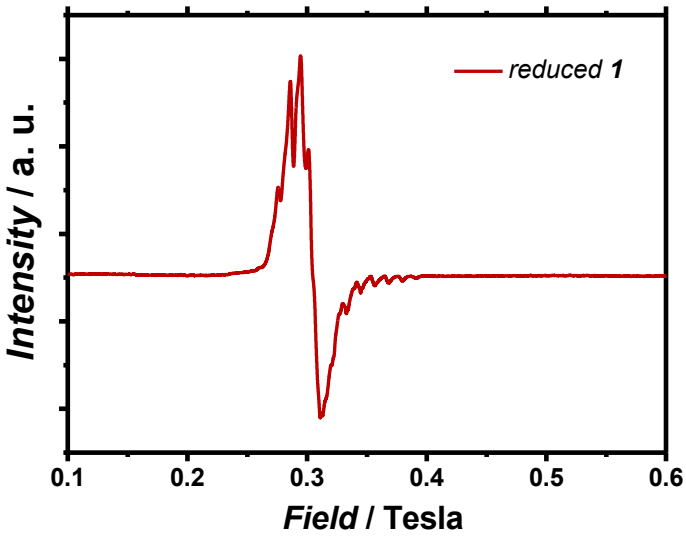

Figure S 22. CW EPR spectra of Co^{II} species obtained by reduction of Cobaloxime 1. The spectrum was recorded in THF solution containing $TBAPF_6$ X-band at temperature 12 K and mw frequency 9.6 GHz.

As it is evident from the spectrum the cobalt (II) complex, in this case it is clearly in a low-spin state as indicated by the hyperfine coupling. The effective *g*-factor was found to be 2.2.

References

1. V. Artero, M. Chavarot-Kerlidou and M. Fontecave, *Angew. Chem. Int. Ed.*, 2011, **50**, 7238-7266.
2. S. Pullen, H. Fei, A. Orthaber, S. M. Cohen and S. Ott, *J. Am. Chem. Soc.*, 2013, **135**, 16997-17003.
3. Y. Horiuchi, T. Toyao, M. Saito, K. Mochizuki, M. Iwata, H. Higashimura, M. Anpo and M. Matsuoka, *J. Phys. Chem. C*, 2012, **116**, 20848-20853.
4. T. Zhou, Y. Du, A. Borgna, J. Hong, Y. Wang, J. Han, W. Zhang and R. Xu, *Energy Environ. Sci.*, 2013, **6**, 3229-3234.
5. A. Fateeva, P. A. Chater, C. P. Ireland, A. A. Tahir, Y. Z. Khimyak, P. V. Wiper, J. R. Darwent and M. J. Rosseinsky, *Angew. Chem. Int. Ed.*, 2012, **51**, 7440-7444.
6. C. Wang, K. E. Dekrafft and W. Lin, *J. Am. Chem. Soc.*, 2012, **134**, 7211-7214.
7. P. Zhang, P.-A. Jacques, M. Chavarot-Kerlidou, M. Wang, L. Sun, M. Fontecave and V. Artero, *Inorg. Chem.*, 2012, **51**, 2115-2120.
8. S. Varma, C. E. Castillo, T. Stoll, J. Fortage, A. G. Blackman, F. Molton, A. Deronzier and M.-N. Collomb, *Phys. Chem. Chem. Phys.*, 2013, **15**, 17544-17552.
9. M. Guttentag, A. Rodenberg, R. Kopelent, B. Probst, C. Buchwalder, M. Brandstätter, P. Hamm and R. Alberto, *Eur. J. Inorg. Chem.*, 2012, **2012**, 59-64.
10. K. T. Butler, C. H. Hendon and A. Walsh, *J. Am. Chem. Soc.*, 2014, **136**, 2703-2706.
11. C. H. Hendon, D. Tiana, M. Fontecave, C. Sanchez, L. D'arras, C. Sassoye, L. Rozes, C. Mellot-Draznieks and A. Walsh, *J. Am. Chem. Soc.*, 2013, **30**, 10942-10945.
12. P.-A. Jacques, V. Artero, J. Pécaut and M. Fontecave, *Proc. Natl. Acad. Sci. U.S.A.*, 2009, **106**, 20627-20632.
13. S. Stoll and A. Schweiger, *J. Magn. Reson.*, 2006, **178**, 42-55.
14. S. Stoll and A. Schweiger, *Biol. Magn. Reson.*, 2007, **27**, 299-321.
15. A. Bencini, I. Bertini, G. Canti, D. Gatteschi and C. Luchinat, *J. Inorg. Biochem.*, 1981, **14**, 81-93.
16. I. Krivokapic, M. Zerara, M. L. Daku, A. Vargas, C. Enachescu, C. Ambrus, P. Tregenna-Piggott, N. Amstutz, E. Krausz and A. Hauser, *Coord. Chem. Rev.*, 2007, **251**, 364-378.